NASA/TM—2000-210208

Mechanical, Chemical and Microstructural Characterization of Monazite-Coated Silicon Carbide Fibers

N.P. Bansal and D.R. Wheeler
Glenn Research Center, Cleveland, Ohio

Y.L. Chen
Dynacs Engineering Company, Inc., Brook Park, Ohio

June 2000

The NASA STI Program Office . . . in Profile

Since its founding, NASA has been dedicated to the advancement of aeronautics and space science. The NASA Scientific and Technical Information (STI) Program Office plays a key part in helping NASA maintain this important role.

The NASA STI Program Office is operated by Langley Research Center, the Lead Center for NASA's scientific and technical information. The NASA STI Program Office provides access to the NASA STI Database, the largest collection of aeronautical and space science STI in the world. The Program Office is also NASA's institutional mechanism for disseminating the results of its research and development activities. These results are published by NASA in the NASA STI Report Series, which includes the following report types:

- TECHNICAL PUBLICATION. Reports of completed research or a major significant phase of research that present the results of NASA programs and include extensive data or theoretical analysis. Includes compilations of significant scientific and technical data and information deemed to be of continuing reference value. NASA's counterpart of peer-reviewed formal professional papers but has less stringent limitations on manuscript length and extent of graphic presentations.

- TECHNICAL MEMORANDUM. Scientific and technical findings that are preliminary or of specialized interest, e.g., quick release reports, working papers, and bibliographies that contain minimal annotation. Does not contain extensive analysis.

- CONTRACTOR REPORT. Scientific and technical findings by NASA-sponsored contractors and grantees.

- CONFERENCE PUBLICATION. Collected papers from scientific and technical conferences, symposia, seminars, or other meetings sponsored or cosponsored by NASA.

- SPECIAL PUBLICATION. Scientific, technical, or historical information from NASA programs, projects, and missions, often concerned with subjects having substantial public interest.

- TECHNICAL TRANSLATION. English-language translations of foreign scientific and technical material pertinent to NASA's mission.

Specialized services that complement the STI Program Office's diverse offerings include creating custom thesauri, building customized data bases, organizing and publishing research results . . . even providing videos.

For more information about the NASA STI Program Office, see the following:

- Access the NASA STI Program Home Page at *http://www.sti.nasa.gov*

- E-mail your question via the Internet to help@sti.nasa.gov

- Fax your question to the NASA Access Help Desk at (301) 621-0134

- Telephone the NASA Access Help Desk at (301) 621-0390

- Write to:
  NASA Access Help Desk
  NASA Center for AeroSpace Information
  7121 Standard Drive
  Hanover, MD 21076

NASA/TM—2000-210208

Mechanical, Chemical and Microstructural Characterization of Monazite-Coated Silicon Carbide Fibers

N.P. Bansal and D.R. Wheeler
Glenn Research Center, Cleveland, Ohio

Y.L. Chen
Dynacs Engineering Company, Inc., Brook Park, Ohio

National Aeronautics and
Space Administration

Glenn Research Center

June 2000

Acknowledgments

Thanks are due to Dan Gorican for fiber strength measurements and John Setlock for SEM analysis. We are grateful to Paul Chayka of Advanced Technology Materials, Inc. for coating the fibers with monazite.

Available from

NASA Center for Aerospace Information
7121 Standard Drive
Hanover, MD 21076
Price Code: A03

National Technical Information Service
5285 Port Royal Road
Springfield, VA 22100
Price Code: A03

MECHANICAL, CHEMICAL AND MICROSTRUCTURAL CHARACTERIZATION OF MONAZITE-COATED SILICON CARBIDE FIBERS

N.P. Bansal and D.R. Wheeler
National Aeronautics and Space Administration
Glenn Research Center
Cleveland, Ohio 44135

Y.L. Chen
Dynacs Engineering Company, Inc.
Glenn Research Center
Brook Park, Ohio 44142

SUMMARY

Tensile strengths of as-received Hi-Nicalon and Sylramic fibers and those having monazite surface coatings, deposited by atmospheric pressure chemical vapor deposition, were measured at room temperature and the Weibull statistical parameters determined. The average tensile strengths of uncoated Hi-Nicalon and Sylramic fibers were 3.19±0.73 and 2.78±0.53 GPa with a Weibull modulus of 5.41 and 5.52, respectively. The monazite-coated Hi-Nicalon and Sylramic fibers showed strength loss of ~10 and 15 percent, respectively, compared with the as-received fibers. The elemental compositions of the fibers and the coatings were analyzed using scanning Auger microprobe and energy dispersive x-ray spectroscopy. The $LaPO_4$ coating on Hi-Nicalon fibers was approximately stoichiometric and about 50 nm thick. The coating on the Sylramic fibers extended to a depth of about 100 to 150 nm. The coating may have been stoichiometric $LaPO_4$ in the first 30 to 40 nm of the layer. However, the surface roughness of Sylramic fiber made this profile somewhat difficult to interpret. Microstructural analyses of the fibers and the coatings were done by scanning electron microscopy, transmission electron microscopy, and selected area electron diffraction. Hi-Nicalon fiber consists of fine β-SiC nanocrystals ranging in size from 1 to 30 nm embedded in an amorphous matrix. Sylramic is a polycrystalline stoichiometric silicon carbide fiber consisting of submicron β-SiC crystallites ranging from 100 to 300 nm. Small amount of TiB_2 nanocrystallites (~50 nm) are also present. The $LaPO_4$ coating on Hi-Nicalon fibers consisted of a chain of peanut shape particles having monazite-(La) structure. The coating on Sylramic fibers consisted of two layers. The inner layer was a chain of peanut shape particles having monazite-(La) structure. The outer layer was comprised of much smaller particles with a microcrystalline structure.

1. INTRODUCTION

Silicon carbide fibers are being used as reinforcement (refs. 1 to 4) in ceramic matrix composites (CMC). Hi-Nicalon and Sylramic are the most advanced silicon carbide fibers that are commercially available in the form of small diameter multifilament tows. In order to achieve high strength and, in particular, high toughness in fiber-reinforced CMCs, the fiber-matrix interface must be sufficiently weak (refs. 1 to 3) so that an advancing matrix crack can be deflected at the interface by fiber/matrix debonding. This is generally achieved through engineering the interface by application of surface coatings on the fibers. Carbon and BN are the most common interface coatings (refs. 1 to 4) currently being used. Variations of BN, such as pyrolytic boron nitride (p-BN) and silicon-containing pyrolytic boron nitride (p-B(Si)N), have also been tried because of their better stability (ref. 5) than BN. At elevated temperatures, p-B(Si)N shows 1-3 orders of magnitude greater oxidation resistance than p-BN and is also more resistant to moisture containing atmosphere (ref. 5). However, all these coatings have only limited thermo-oxidative stability, particularly at intermediate temperatures. More recently, a number of oxides, including $LaPO_4$ ((La)-monazite, hereinafter referred to as monazite)), have been investigated (refs. 6 to 13) as fiber/matrix interface coatings, especially for oxide/oxide composites. It is, therefore, necessary to know if the application of these surface coatings results in any strength degradation or microstructural changes in SiC fibers. Tensile strengths of Nextel 720™ fibers were degraded by 25 to >50 percent when coated with monazite (ref. 11).

Mechanical, chemical and microstructural characterization of Hi-Nicalon and HPZ fibers having different types of BN and BN/SiC coatings have recently been reported by Bansal et al. (refs. 14 and 15). More recently, monazite is being investigated as an interface coating for silicon carbide fiber reinforced celsian matrix composites by the present author. The primary objective of the present study was to examine the effects of monazite surface coatings on the tensile strength of Hi-Nicalon and Sylramic fibers. Another objective was to carry out chemical and microstructural characterization of the fibers and the coatings. Microstructural analysis was done by scanning electron microscopy (SEM) and transmission electron microscopy (TEM). Elemental compositions and thickness of the fibers and the coatings were determined by scanning Auger microprobe (SAM), energy dispersive x-ray spectroscopy (EDS), and electron microscopy. Room temperature tensile strength was measured and the Weibull statistical parameters determined for coated and uncoated fibers.

2. MATERIALS

Hi-Nicalon fiber from Nippon Carbon Co. and Sylramic fiber from Dow Corning were used in the present study. The properties of the as-received fibers are shown in Table I. Hi-Nicalon fibers consist of β-SiC and a small amount (<1 wt %) of silicon oxycarbide. This fiber also contains 30 to 40 at. % excess carbon, which is also reflected in its low elastic modulus. A large variation (10 to 18 mm) in the fiber diameter was observed with an average value of 13.5 μm, which is in very good agreement with the value of ~14 μm reported by the manufacturer. Sylramic is a polycrystalline stoichiometric silicon carbide fiber with an average diameter of 10 mm. It shows excellent corrosion resistance, oxidation resistance, high thermal conductivity, high modulus, and strength retention up to about 1400 °C. The surface of Sylramic fiber is significantly rougher than that of Hi-Nicalon fiber.

The polyvinyl alcohol (PVA) sizing on the as-received fibers was burned off in a Bunsen burner flame. The fiber tows were continuously coated with monazite at 540 °C by Advanced Technology Materials, Inc. by an atmospheric pressure chemical vapor deposition (CVD) method (ref. 8) followed by annealing at 1000 °C. Single filaments were carefully separated from the fiber tows for testing.

TABLE I. PROPERTIES OF HI-NICALON AND SYLRAMIC FIBERS

Property	Sylramic[a]	Hi-Nicalon[b]
Density, g/cm^3	3.0	2.74
Diameter, μm	10	14
Filaments/tow	800	500
Denier, g/9000m	1600	1800
Tensile strength, GPa	3.4	2.8
Elastic modulus, GPa	386	269
Thermal expansion coefficient, 10^{-6}/K	5.4 (20-1320°C)	3.5 (25-500°C)
Specific heat, J/g-K	0.75	0.67 (25°C) 1.17 (500°C)
Thermal conductivity, W/m-K	40-45	7.77 (25°C) 10.1 (500°C)
Electrical resistivity, ohm-cm		1.4
Chemical composition, wt %	66.6 Si, 28.5 C, 0.8 O, 2.3 B, 2.1 Ti, 0.4 N	63.7 Si, 35.8 C, 0.5 O
C/Si, atomic ratio	1.0	1.3-1.4
Temperature capability, °C	1400	1200

[a]Data from Dow Corning Corporation
[b]Data from Nippon Carbon Co.

3. EXPERIMENTAL

3.1. Electron microscopy

The surfaces of the fibers were examined using SEM and TEM. For cross-sectional analysis, fibers were mounted in a high temperature epoxy and polished before examination. A thin carbon coating was evaporated onto the SEM specimens to provide electrical conductivity prior to analysis. Fiber cross-sectional thin foils for TEM were prepared

using a procedure developed for ceramic fibers which involves epoxy potting, sandwiching, slicing, tripod polishing, and argon ion milling. SEM was performed using a JEOL JSM-840A operating at 15 keV. X-ray elemental analyses were done using a Kevex thin window energy dispersive spectrometer (EDS) and analyzer. The TEM thin foils were examined in a Philips EM200 operating at 120 keV equipped with a Kevex EDS and a Gatan Image Filter (GIF) for elemental analysis.

3.2. Scanning Auger Analysis

3.2.1. Sample Preparation.— Each fiber-tow was cut to about 1cm length. Individual fibers were then extracted from the tow and mounted for depth profiling on a stainless steel surface. The fiber segments were held at each end by a droplet of aqueous colloidal graphite suspension (DAG) which was allowed to dry at a temperature less than 40 °C. The fibers were otherwise untreated before analysis.

3.2.2. Spectroscopy.—Auger Electron Spectroscopy (AES) was performed on a VG Scientific MicroLab 310F scanning Auger microprobe. In the spectrometer, the fiber was tilted at 60° to the electron beam, and a smooth portion of the fiber was imaged at 5 kX magnification. The electron beam energy was 2 keV and the current ~3 nA. During analysis, the electron beam was rastered over an area ~1 by 5 μm along the length of the fiber, and the spectrum of secondary electrons was recorded. The sample tilt, low electron-beam energy and large area of analysis prevented the sample from charging and distorting the secondary electron spectrum.

The raw data consisted of the areas under features in the spectrum corresponding to the elements present. These areas were converted to atomic percent by dividing by empirical sensitivity factors and normalizing the results to total 100 percent. The sensitivity factors were determined from the spectra of standard materials after Ar-ion etching. The etching was necessary to take into account the differential sputter rate of different elements in a compound. These sensitivity factors were thus characteristic of the sputter-etched materials. However, the effect of differential sputtering is dependent on the structure and precise stoichiometry of the material as well as other factors. Thus the effect may be different in the standards and the materials analyzed. Therefore, the values of atomic-percent reported here are subject to inevitable uncertainties of at least 5 percentage points.

Depth profiles (plots of composition versus depth below the material surface) were acquired by repeated cycles of analysis and Ar ion-beam etching to remove material. The ion-beam energy was 3 keV, the beam current was 500 nA and the beam was rastered over an area ~2 by 2 mm. The etch rate under these conditions was measured by etching a 100 nm thick Ta_2O_5 film, and found to be 0.04 nm/s. All the depth profiles shown have a depth scale determined by multiplying the etch time by that rate. The depths reported are therefore only nominal values, since the etch rate will vary from one material to another, however a comparison of depths in the same material is valid.

An important factor in interpreting depth profiles is the depth-resolution of the technique. An atomically flat interface would not appear that way in a depth profile for two reasons. First, the electron spectrum, while sensitive to the outermost atomic layer of a surface, also has a contribution from layers below. The contributing depth depends on the particular energy being analyzed but can be 3 to 10 nm. Secondly, the process of ion-etching disrupts the surface region, effectively homogenizing a layer with a thickness that generally increases with etching depth, being 5 to 10 percent of the depth in our case. In addition, the ion etch rate depends on the angle of incidence of the ion beam. Therefore, on rough surfaces, there will be a range of etch rates which will contribute to a "smearing" of features that will increase as the depth increases. In the present instance this may be important in the profile of the Sylramic fiber which has significant roughness.

3.3. Tensile Strength Measurements

Room temperature tensile strengths of the individual filaments were measured in ambient atmosphere with a screw driven Micropull fiber test frame equipped with pneumatic grips [16]. A 1000 g load cell, Sensotec model 34, was used. Measurements were carried out at a constant crosshead speed of 1.261 mm/min (0.05 in./min). A single filament was mounted on a picture frame shaped paper tab using Hardman extra fast setting epoxy. The side portions of the tab were cut with a hot wire just before application of the load producing a fiber gage length of 2.54 cm (1 in.). Twenty filaments of each type of fiber were tested. Weibull parameters for tensile strength of fibers were calculated based on an average fiber diameter of 13.5 μm for Hi-Nicalon and 10.8 μm for Sylramic.

4. RESULTS AND DISCUSSION

4.1. Electron Microscopic Analysis

4.1.1. Hi-Nicalon fiber.—SEM micrographs showing the surface of as-received, flame desized Hi-Nicalon fibers are presented in figure 1. The fiber surface appears to be fairly smooth and featureless. EDS compositional spectra (fig. 2) taken from the polished cross-section of the fiber indicate the presence of only Si and C along with a small amount of oxygen which is in qualitative agreement with the manufacturer's data (table I). A pair of TEM bright-field (a) and dark-field (b) images from Hi-Nicalon fiber along with the selected-area diffraction pattern (SADP) shown as the inset are given in figure 3. These results indicate that Hi-Nicalon fiber consists of a SiC nano-crystalline structure, i.e., fine β-SiC crystallites (white features in dark-field) of size ranging from 1 to 30 nm which are imbedded in an amorphous matrix, probably carbon. The apparent mean grain size of the β-SiC crystallites calculated from the width of the (111) X-ray diffraction peak at mid-height using the Scherrer equation has been reported (refs. 17 and 18) to be about 3 to 5 nm. No peak assigned to turbostratic carbon was observed (ref. 17) in the X-ray diffraction.

4.1.2. Hi-Nicalon/$LaPO_4$ fiber.—SEM micrographs taken from the surface of monazite coated Hi-Nicalon fibers are given in figure 4. The coating on most of the fibers is generally uniform and smooth. However, some fibers have a very thick and nonuniform coating (fig. 4(b)). TEM bright-field image of the monazite-coated Hi-Nicalon fiber is shown in figure 5(a). The coating consists of a chain of peanut shape particles with an average thickness of 20 nm, which is much thinner than the coating of Sylramic fiber. Microdiffraction (fig. 5(b)) and EDS (fig. 5(d)) analysis show that the peanut shape particles have the monazite-(La) structure, i.e., $LaPO_4$. SADP (fig. 5(c)) from the fiber indicates its nanocrystalline structure. The high-resolution images (fig. 6) show the interface between fiber and coating, where figure 6(b) is the interface between fiber and a monazite crystallite and figure 6(a) is the interface between the fiber and the amorphous region between two monazite crystallites. The amorphous region is high in oxygen and low in lanthanum as indicated by EDS in figure 5(e) and elemental maps using GIF in figure 7. Figure 7(a) is the bright-field image of the fiber and coating where elemental maps of carbon (fig. 7(b)), lanthanum (fig. 7(c)) and oxygen (fig. 7(d)) were taken. In the elemental maps, the bright area indicates the particular element rich region. The results obtained by comparison of the elemental dot maps in figure 7 are in agreement with the EDS data, i.e., the amorphous area between the monazite crystallites is richer in oxygen and poorer in lanthanum than the monazite.

4.1.3. Sylramic fiber.—An SEM micrograph showing the surface of as-received, flame desized Sylramic fibers is presented in figure 8. The fiber surface appears to be fairly smooth and featureless. The diameter of Sylramic fiber ranged from 8 to 10 μm. The selected-area electron diffraction pattern (SADP) in figure 9(b) and EDS analysis in figure 9(c) indicate that this fiber consists of a SiC polycrystalline structure. The size of the SiC crystallites range from 100 to 300 nm, as seen from the bright-field image (Fig. 9(a)). Small amounts of oxygen and titanium were also detected from EDS analysis (fig. 9(c)) of the fiber. The small particles of average size 50 nm (some of which are marked by arrows) in the TEM bright-field image (fig. 9(a)) were identified as TiB_2 crystallites from EDS (fig. 9(d)) and microdiffraction analyses.

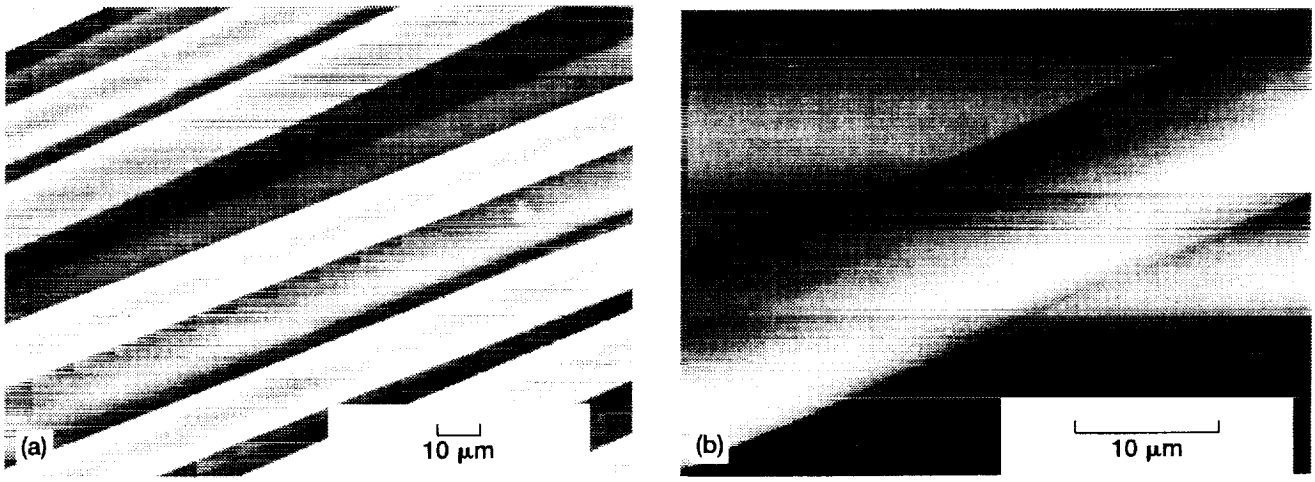

Figure 1.—SEM micrographs (a) and (b) showing surface of desized Hi-Nicalon fibers.

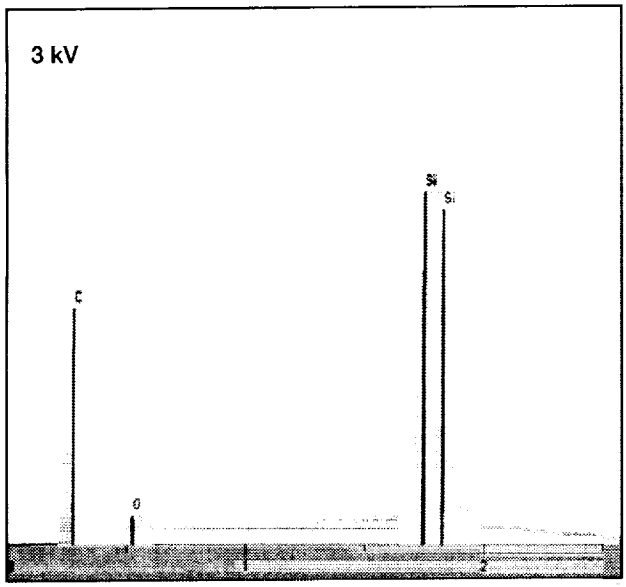

Figure 2.—EDS spectra from the cross-section of desized Hi-Nicalon fiber at 3 kV.

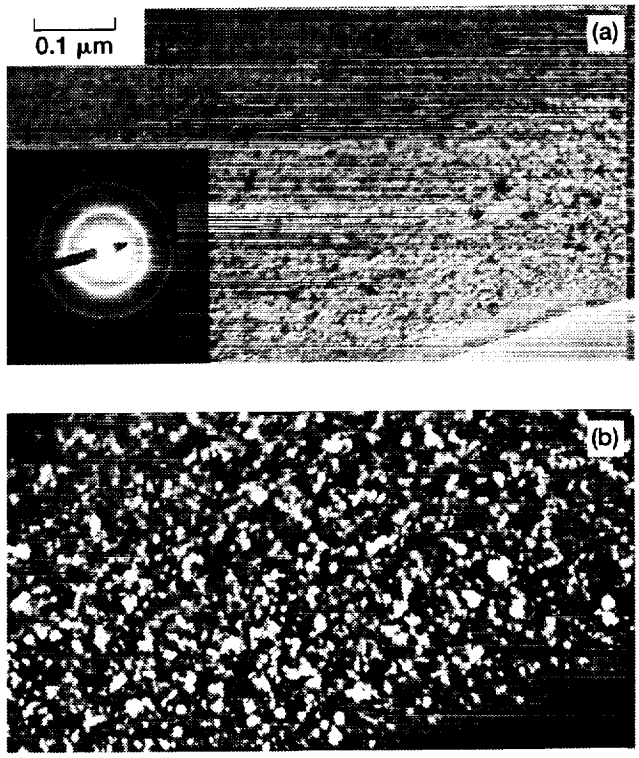

Figure 3.—Pair of TEM bright-field (a) and dark-field (b) images from desized Hi-Nicalon fiber. The SADP is shown as inset.

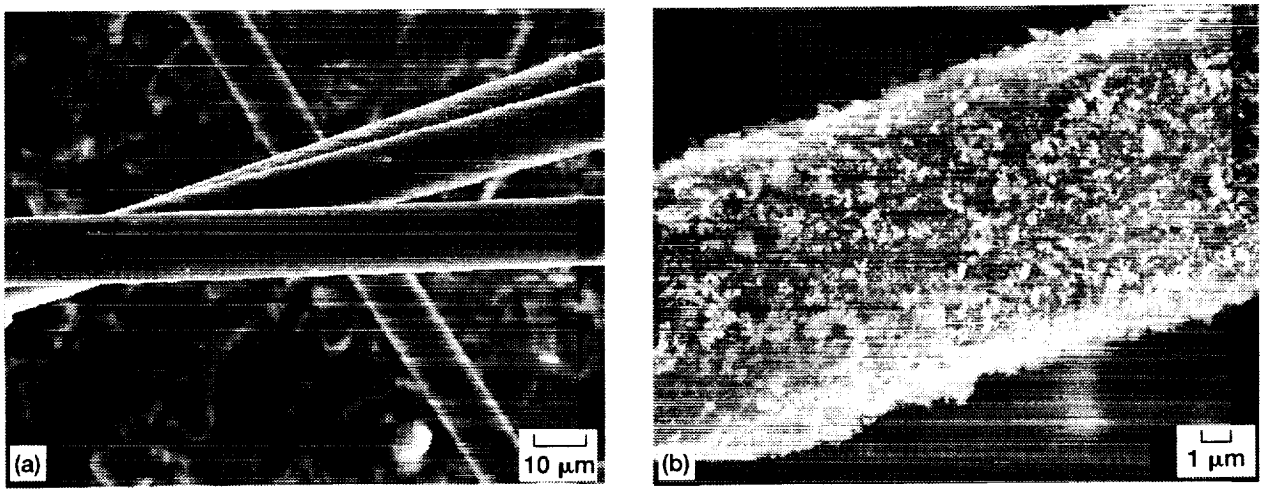

Figure 4.—SEM micrographs (a) and (b) from surface of $LaPO_4$ coated Hi-Nicalon fibers showing large differences in coating thickness.

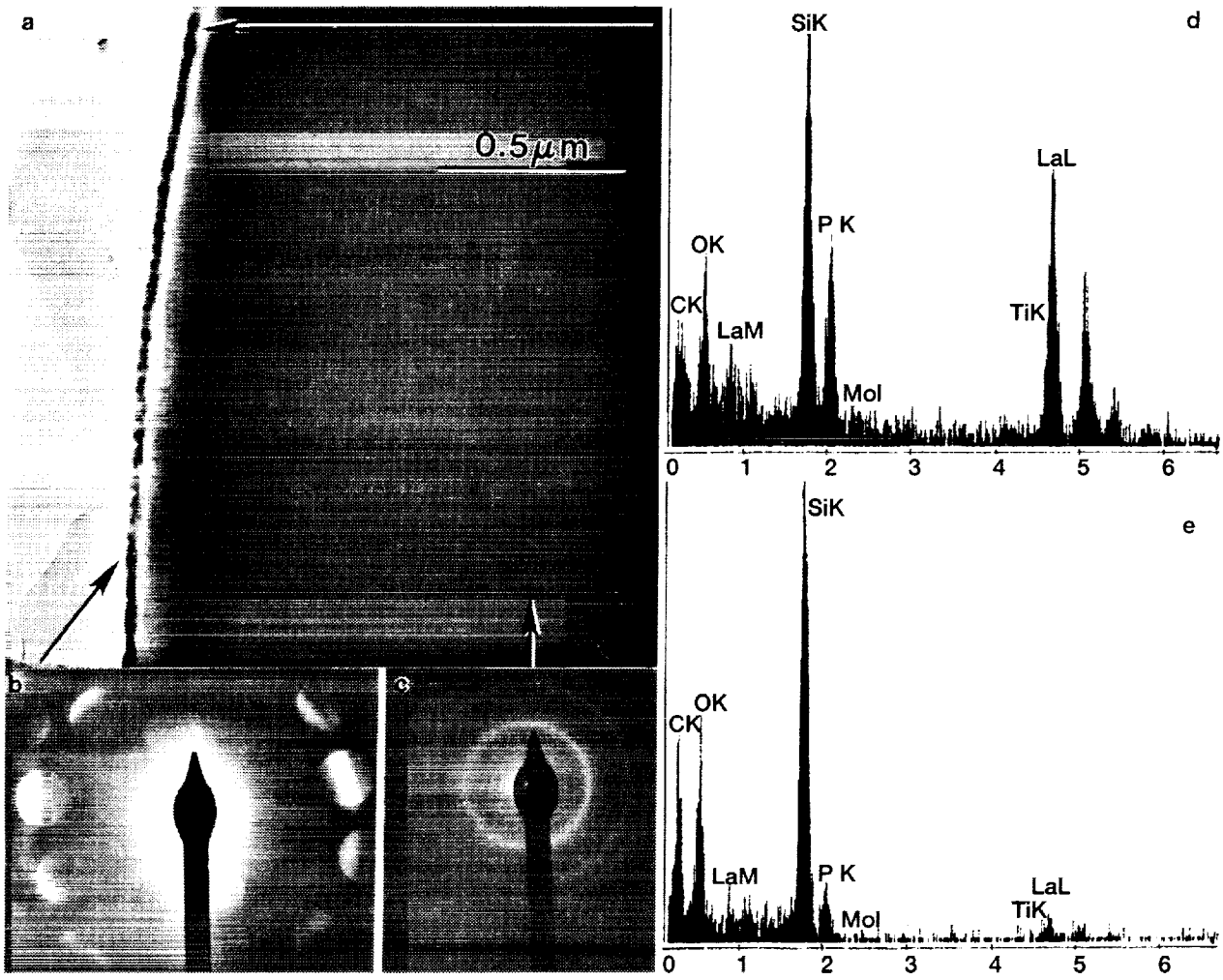

Figure 5.— TEM cross-sectional image (a) of the monazite-coated Hi-Nicalon fiber, electron micro-diffraction pattern from one of the monazite crystallites (b), SADP from the fiber (c), EDS from the monazite cystrallites (d) and the amorphous region (e) between the monazite crystallites.

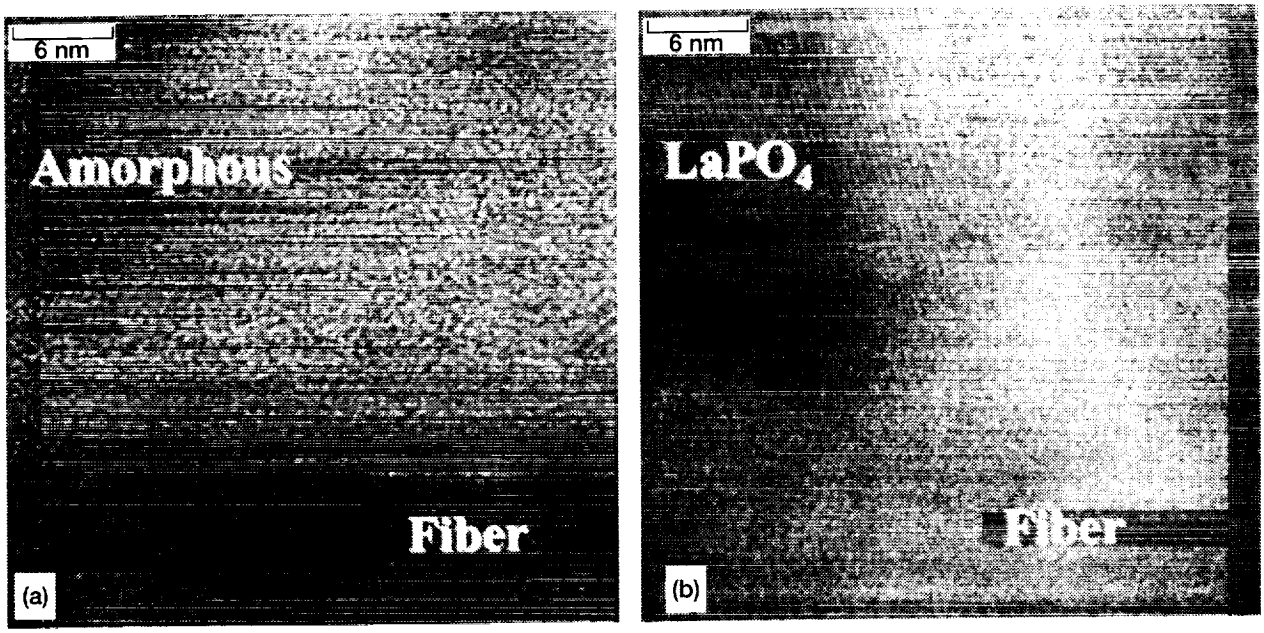

Figure 6.—TEM high resolution images from the interface between the Hi-Nicalon fiber and the amorphous region of the coating (a) and the interface between the Hi-Nicalon fiber and the monazite crystallite of the coating (b).

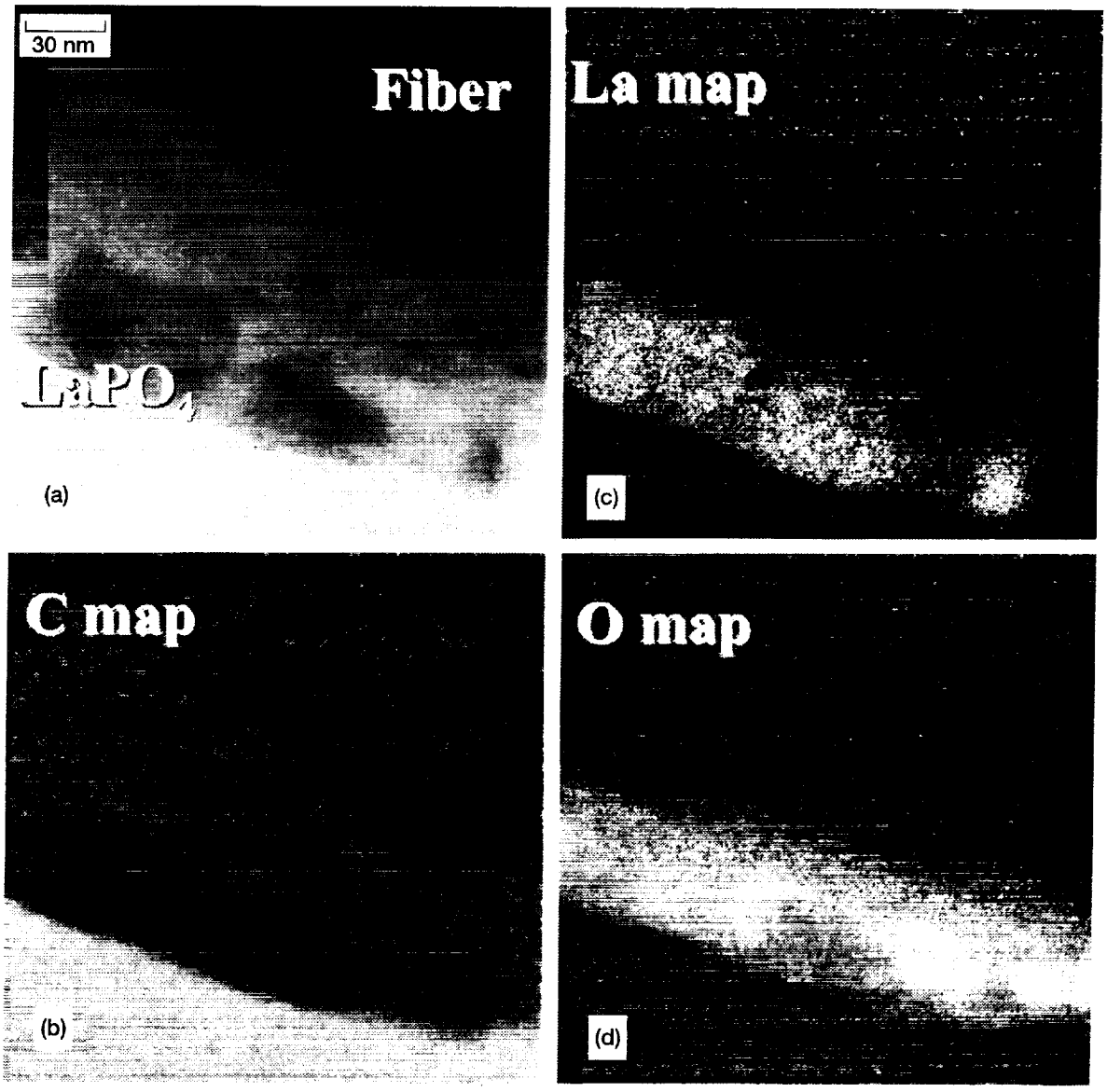

Figure 7.—TEM bright-field image of the monazite-coated Hi-Nicalon fiber (a) and the corresponding GIF elemental maps of carbon (b), lanthanum (c) and oxygen (d).

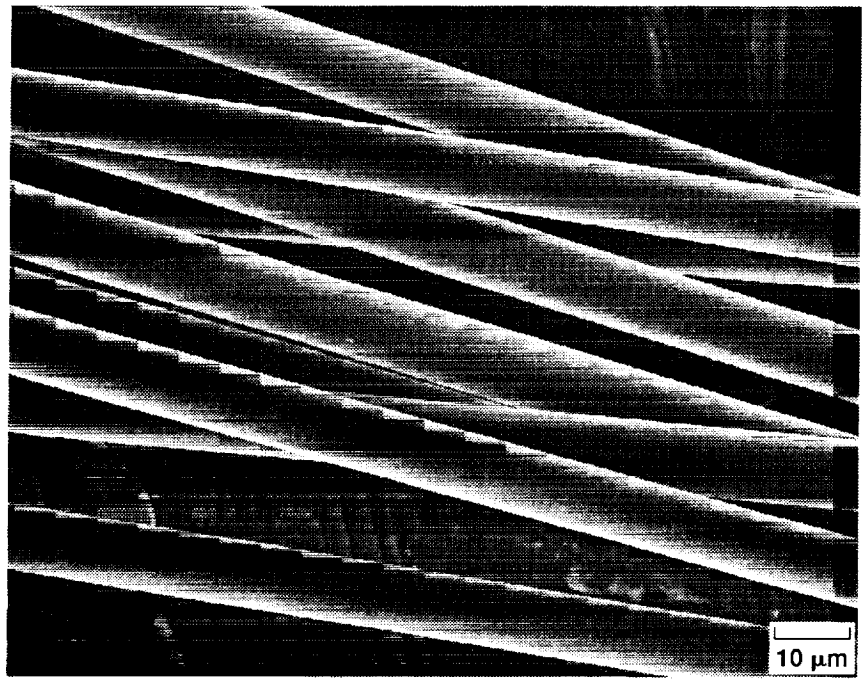

Figure 8.—SEM micrograph showing surface of desized Sylramic fibers.

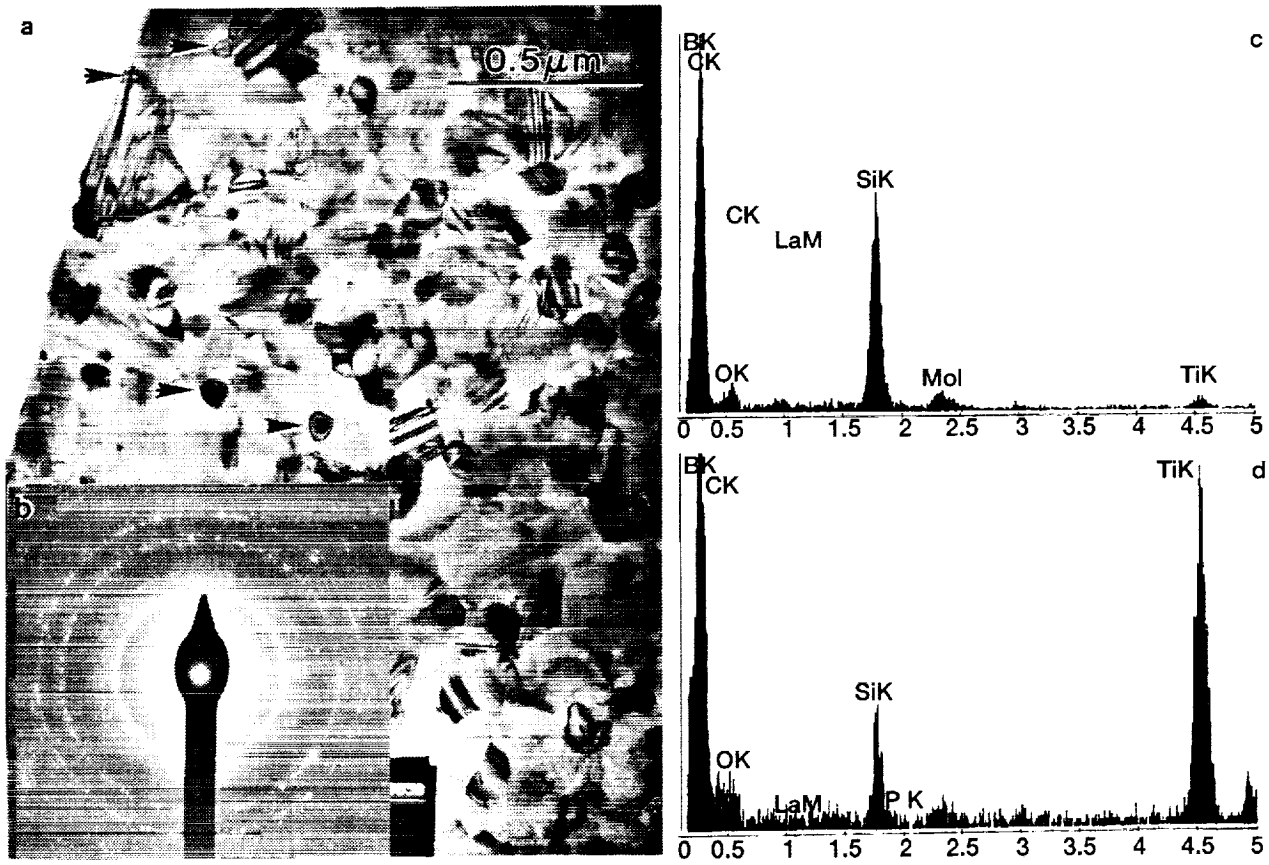

Figure 9.—TEM cross-sectional image of the Sylramic fiber (a), SADP from the fiber (b), EDS from the fiber (c) and the TiB_2 particle (d), respectively.

4.1.4 Sylramic/$LaPO_4$ fiber.— An SEM micrograph showing the surface of monazite coated Sylramic fiber is presented in figure 10. The coating quality varies from smooth, thin and uniform to granular, thick and defective. The coating appears to have cracked on some of the filaments. A bright-field image of the monazite-coated Sylramic fiber is shown in figure 11(a). The fiber surface coating consists of two layers. The inner layer is a chain of peanut shape particles (average thickness 100 nm and length 200 nm) and the outer layer consists of much smaller (average 30 nm) particles. The outer coating varies in thickness and was as thick as 500 nm. Electron microdiffraction (fig. 11(b)) and EDS (fig. 11(d)) analyses indicate that the peanut shape particles consist of monazite-(La) structure, i.e., $LaPO_4$. No significant differences could be observed in the compositions of the inner and outer layers of the coating from EDS analyses (figs. 11(d) and (e)). TEM micrograph of the two-layer coating and fiber area (fig. 12(a)) and the corresponding La map (fig. 12(b)) indicates high lanthanum content in both the outer coating and the peanut shape monazite crystallites of the inner coating, but low La in the amorphous region of the inner coating. However the SADP from the outer coating (fig. 11(c)) indicates a different crystalline structure: a microcrystalline structure, as also shown in the high-resolution image in figure 13.

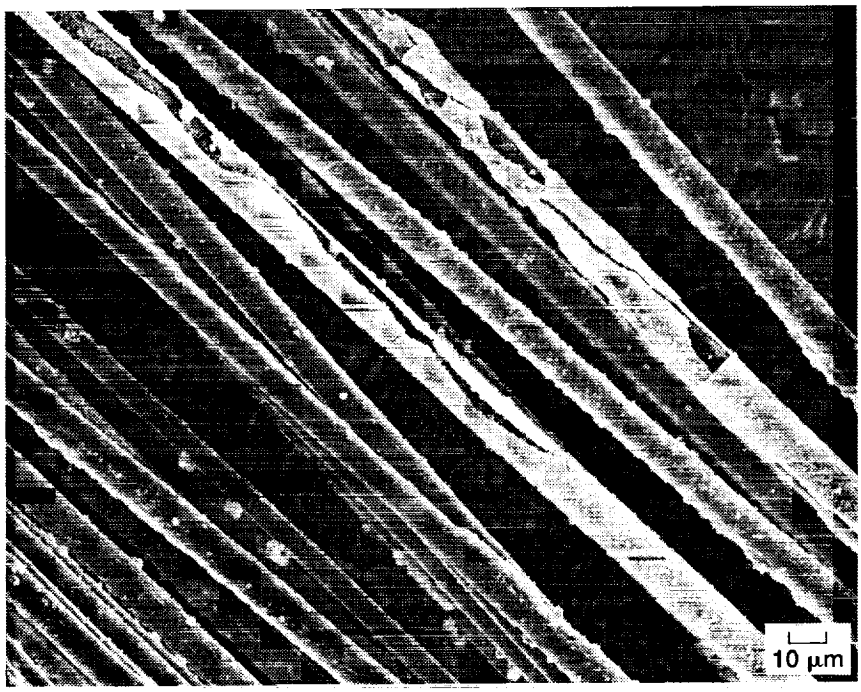

Figure 10.—SEM micrograph from surface of monazite-coated Sylramic fiber.

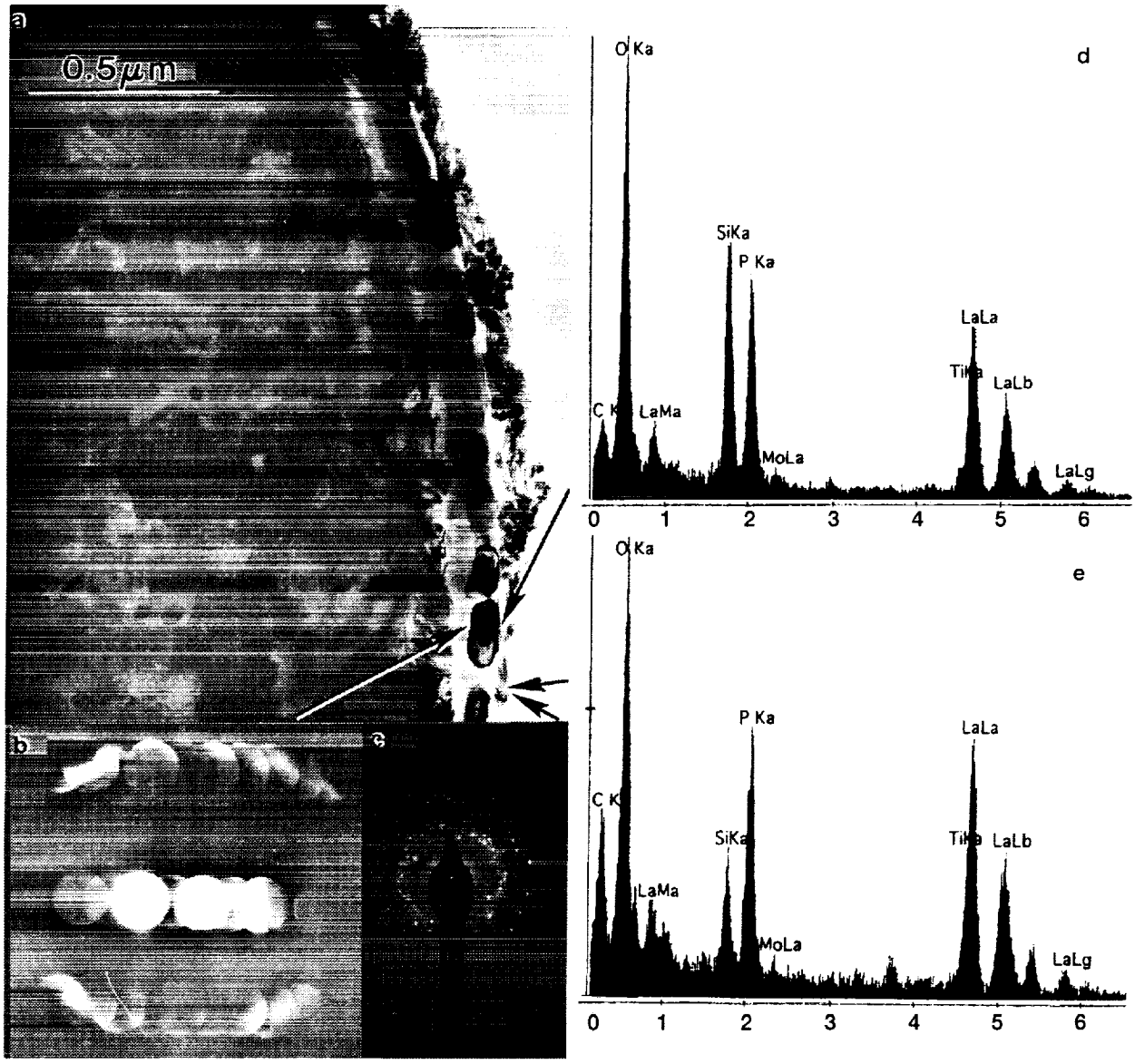

Figure 11.—TEM cross-sectional image (a) of the monazite-coated Sylramic fiber, microdiffraction pattern from one of the monazite crystallites in the inner layer (b), SADP from the outer layer (c), EDS from the monazite crystallites in the inner layer (d) and the outer layer (e).

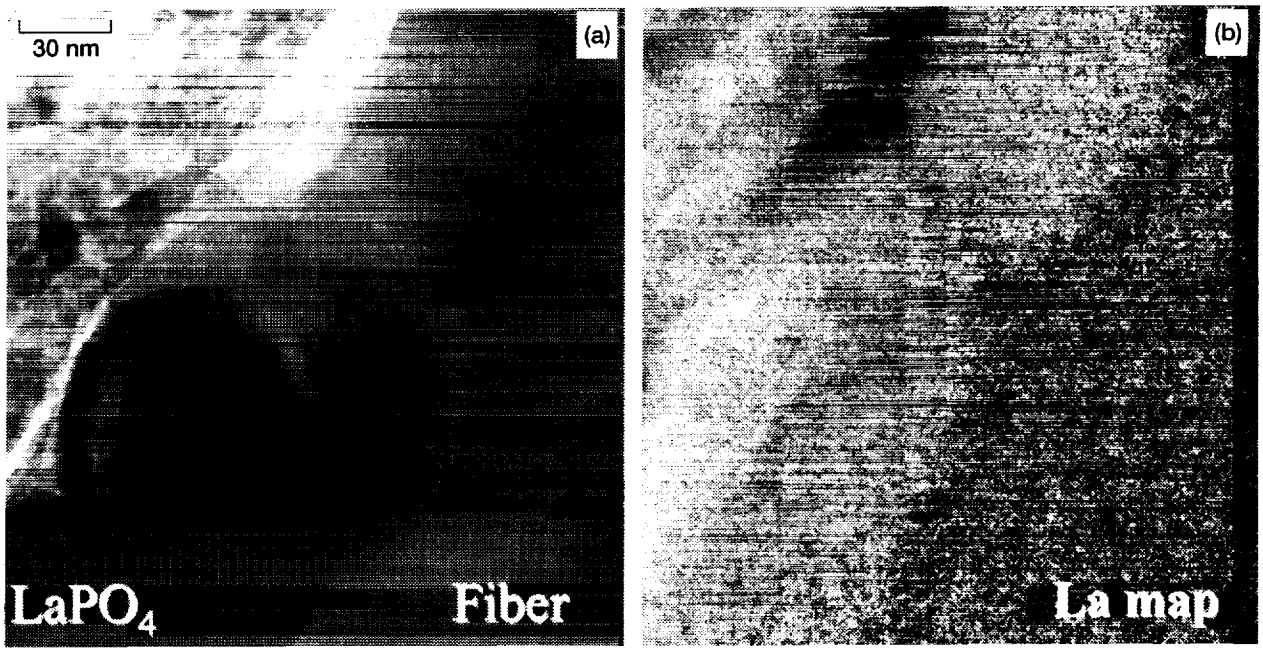

Figure 12.—TEM bright-field image of monazite-coated Sylamic fiber (a) and the corresponding GIF elemental map of lanthanum (b).

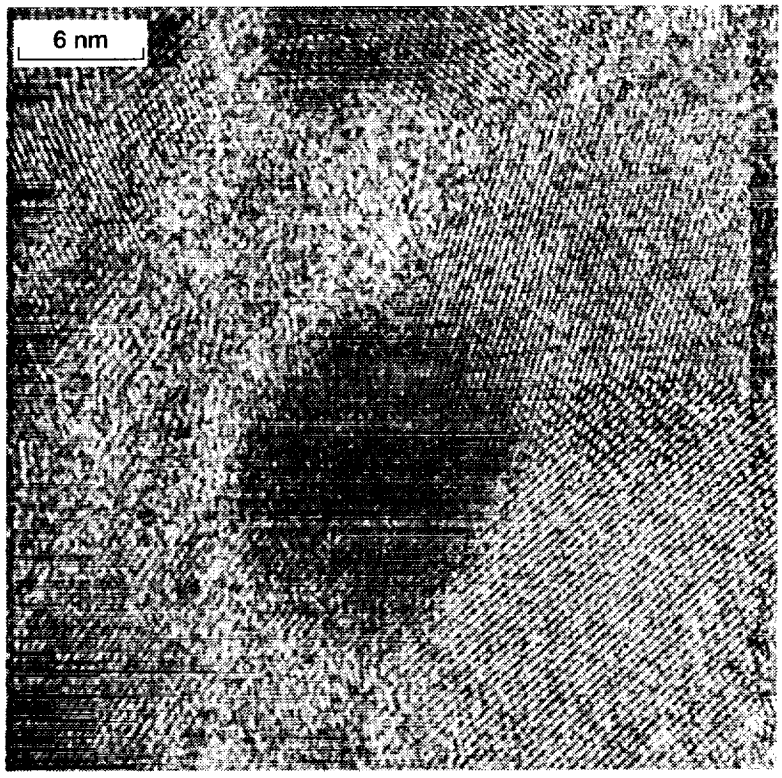

Figure 13.—TEM high resolution image from the micro-crystallite structural outer layer of the coating in the monazite-coated Sylramic fiber.

4.2. Scanning Auger Analysis

Elemental composition depth profiles, as obtained from scanning Auger analysis of as-received, but desized, Hi-Nicalon and Sylramic fibers and those having monazite surface coatings are shown in figure 14.

4.2.1 Hi-Nicalon fiber.—The elemental composition (atomic %) of the as-received fiber (fig. 14(a)) is ~42 % Si and 56% C with C/Si atomic ratio of 1.33. A trace amount of oxygen is also detected. These results are in good agreement with the fiber composition supplied by the manufacturer (table I).

4.2.2 Sylramic fiber.—A high C concentration is seen (fig. 14(b)) at the surface, which may be due to contamination found on any material, and can be disregarded. This could also be from the residue left behind from the PVA sizing on the fiber. Below a depth of ~10 nm, Si and C are present in almost 1:1 ratio, required for stoichiometric SiC in the fiber. Ti and B are also detected that confirms the presence of TiB_2 in the fiber. Trace amount of N is also detected.

4.2.3 Hi-Nicalon/$LaPO_4$ fiber.—There are three regions of interest in the profile (fig. 14(c)): the coating – roughly the La containing region, the fiber – the region in which the Si and C concentrations were stable and the interfacial region, between these two. The $LaPO_4$ coating extended to a depth of about 50 nm and was approximately stoichiometric. Although there appeared to be excess La, the limits of the quantification procedure make this highly uncertain. In the interfacial region from about 55 to 75 nm, concentrations changed rapidly. This region was impossible to quantify accurately because of the depth resolution effects mentioned above, but it is clear that La disappears, P increased and there was excess C. Oxygen was probably present, but because of its steep gradient, it was hard to quantify. Finally, below about 80 nm the Hi-Nicalon fiber appeared. Excess C is characteristic of these fibers.

4.2.4 Sylramic/$LaPO_4$ fiber.—Again, there are three other regions of interest in the profile (fig. 14(d)): the coating – roughly the La containing region, the fiber – the region in which the Si and C concentrations were stable and the interfacial region, between these two. The effect of surface roughness of this fiber on depth resolution, which was mentioned above, made it difficult to interpret this profile. There may have been a stoichiometric $LaPO_4$ layer in the first 30 to 40 nm, and there was clearly excess P in the interfacial region. It also appears that C increased before Si in the 50 to 80 nm region below the surface. All of this could be consistent with a coating identical to that on the Hi-Nicalon fiber, but with a profile distorted by the roughness of the Sylramic fiber. In the fiber itself, below 250 nm, the profile showed only Si and C with a Si:C ratio of 1:1, as expected.

4.3. Tensile Strength

Ceramic fiber strength is determined by the statistical distribution of flaws in the material. The tensile strength of ceramic fibers is generally analyzed on the basis of the well known Weibull statistics (ref. 19). An excellent review of the subject was provided by Van der Zwaag (ref. 20). The Weibull modulus describes the distribution of strength in materials, which fail at defects according to the weakest link statistics. The probability of survival of a material is given by the empirical equation:

$$P_s = 1 - P(\sigma) = \exp\left[-V\left\{(\sigma - \sigma_u)/\sigma_o\right\}^m\right] \qquad (1)$$

where P_s is the survival probability ($P(s) = 1 - P_s$ is the failure probability) of an individual fiber at an applied stress of σ, V is the fiber volume, σ_u is the stress below which failure never occurs, σ_o is the scale parameter, and m is the shape or flaw dispersion parameter. For a given material, the Weibull modulus m and σ_o are constant. Assuming $\sigma_u = 0$ and uniform fiber diameter along the length, L, corresponding to the volume, V, equation (1) can be rearranged as:

$$\ln\ln\left(1/P_s\right) = \ln\ln\left[1/(1/P(\sigma))\right] = m\ln\sigma + \text{constant} \qquad (2)$$

The experimental data are ranked in ascending order of strength values and the cumulative probability $P(\sigma_i)$ is assigned as

$$P(\sigma_i) = i/(1+N) \qquad (3)$$

where i is the rank of the tested fiber in the ranked strength tabulation and N is the total number of fibers tested. A least-squares linear regression analysis is then applied to a plot of $\ln\ln 1/P_s$ versus $\ln(\sigma)$ whose slope is the Weibull modulus m.

It has recently been reported (refs. 15 and 21) that the strength and Weibull modulus of ceramic fibers obtained using measured and average values of fiber diameters were in good agreement. Therefore, an average fiber diameter of

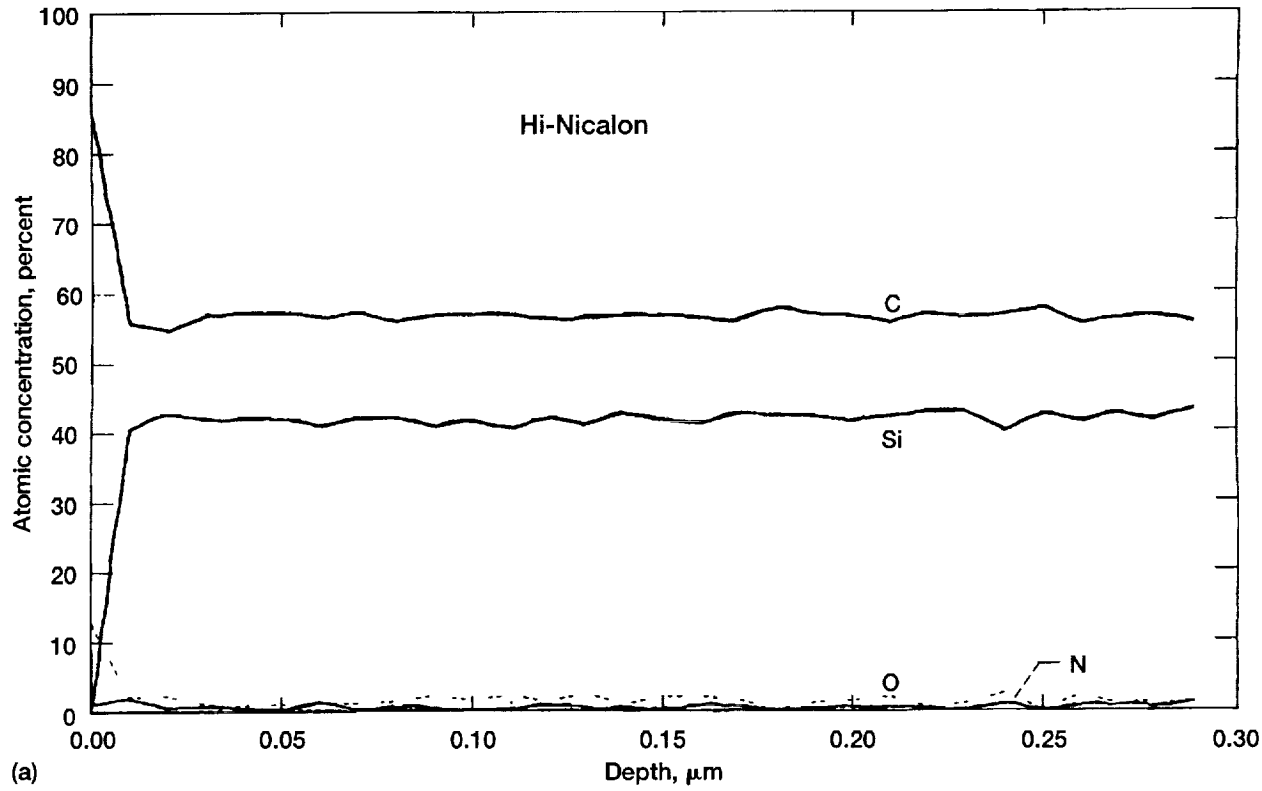

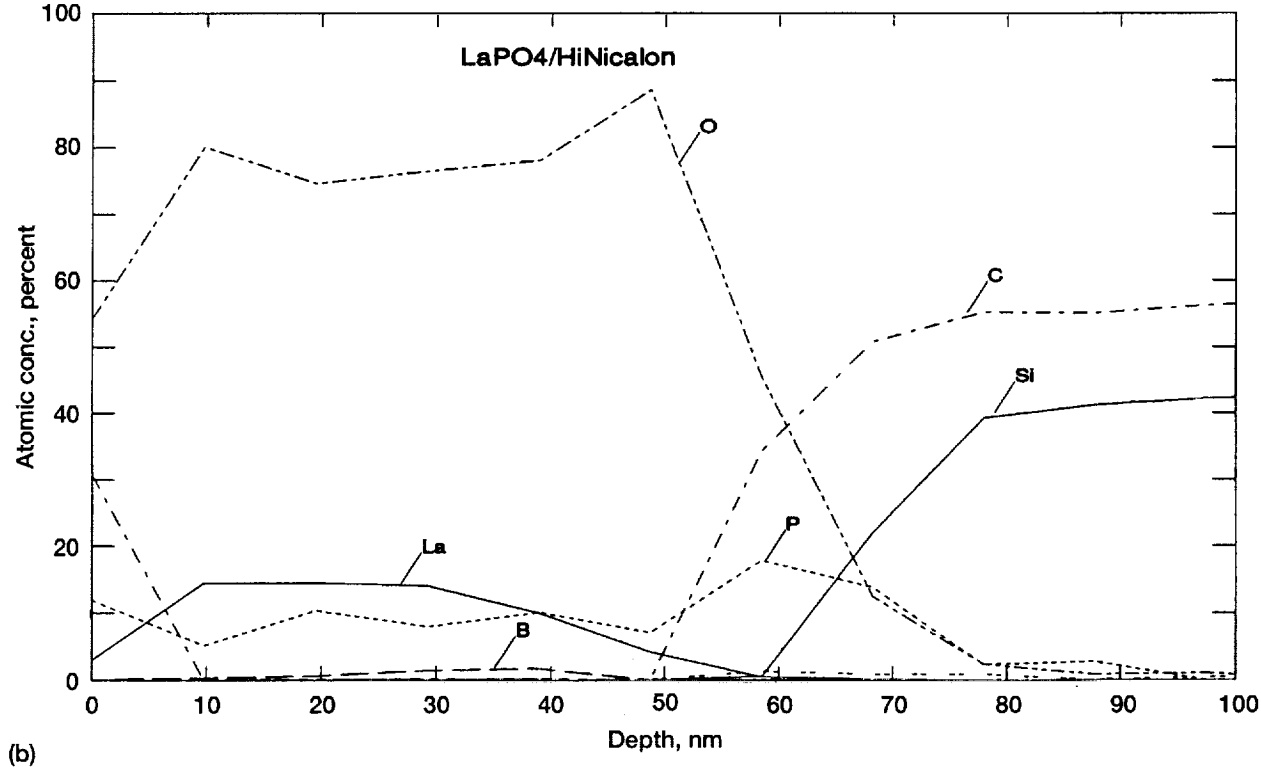

Figure 14.—Surface depth profiles of various elements obtained using scanning Auger microprobe for (a) Hi-Nicalon, (b) Hi-Nicalon/$LaPO_4$, (c) Sylramic, and (d) Sylramic/$LaPO_4$ fibers.

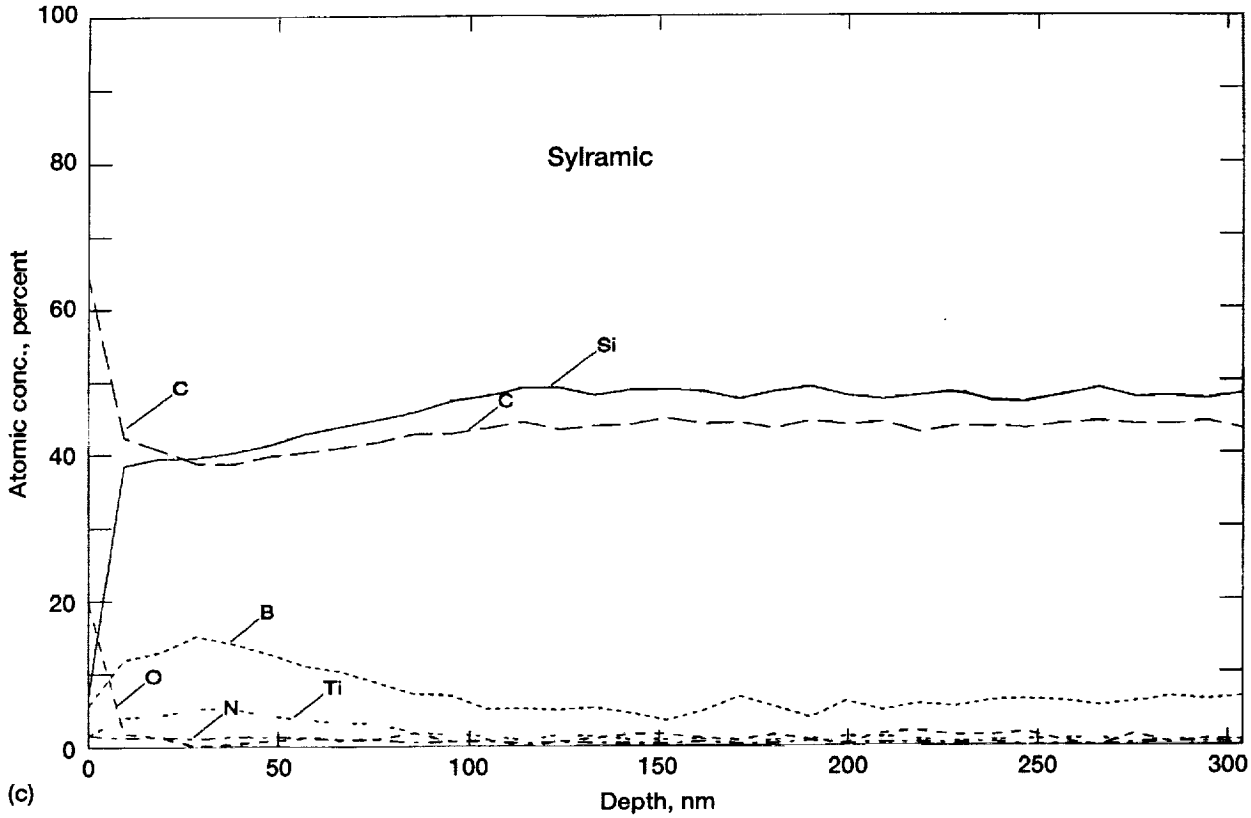

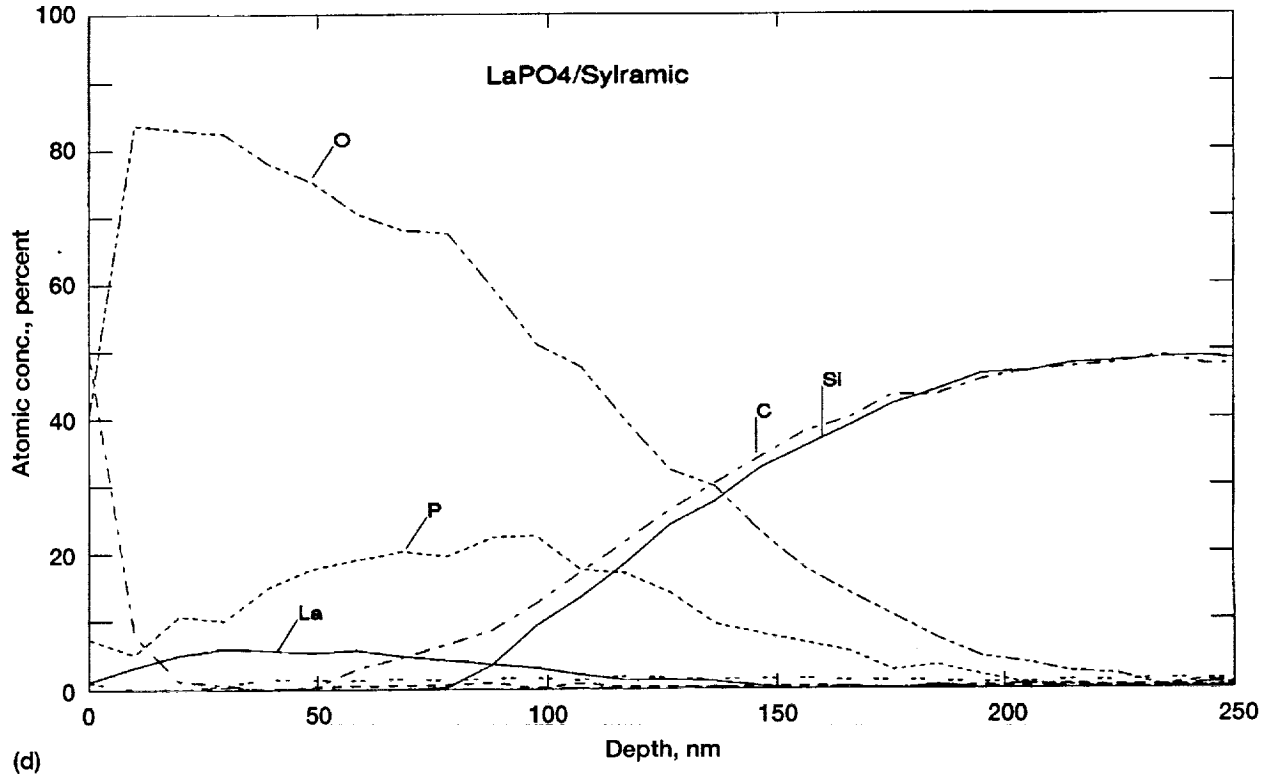

Figure 14.—Concluded. (c) Sylramic, and (d) Sylramic/$LaPO_4$ fibers.

13.5 μm for Hi-Nicalon and 10.8 μm for Sylramic, instead of the measured diameter for each filament, was used in calculating strength and Weibull modulus of fibers in the present study. For the coated fibers, the coating was excluded from fiber diameter measurements, as monazite is not strongly bonded to the fiber surface. The ln ln $(1/P_s)$ versus ln σ Weibull probability plots for room temperature tensile strength of uncoated and $LaPO_4$ coated Hi-Nicalon and Sylramic fibers are presented in figure 15 and the values of Weibull parameters obtained from linear regression analysis are summarized in table II. For the as-received Hi-Nicalon and Sylramic fibers, values of tensile strength are 3.19±0.73 and 2.78±0.53 GPa and Weibull modulus are 5.41 and 5.52, respectively. Hurst et al. measured (ref. 22) tensile strength of seven different lots of Hi-Nicalon fiber. The room temperature strength varied from 2.7 to 3.6 GPa with an average value of 3.0 GPa. The Weibull modulus ranged from 7 to 9. For the Sylramic fiber, room temperature tensile strength varied from 2.1 to 4.3 GPa. The Weibull modulus ranged from 4 to 6. The manufacturer's information data sheets (ref. 23) report room temperature tensile strength values of 2.8 GPa for Hi-Nicalon and 3.4 GPa for Sylramic fibers. The Hi-Nicalon and Sylramic fibers coated with monazite surface layers show strength loss of ~10 and 15 percent, respectively. It has also been recently reported (ref. 11) that tensile strengths of Nextel 720™ fibers were degraded by 25 to >50 percent when coated with monazite using different precursors. This reduction in strength has been attributed to stress corrosion from different decomposition products from various precursor chemistries.

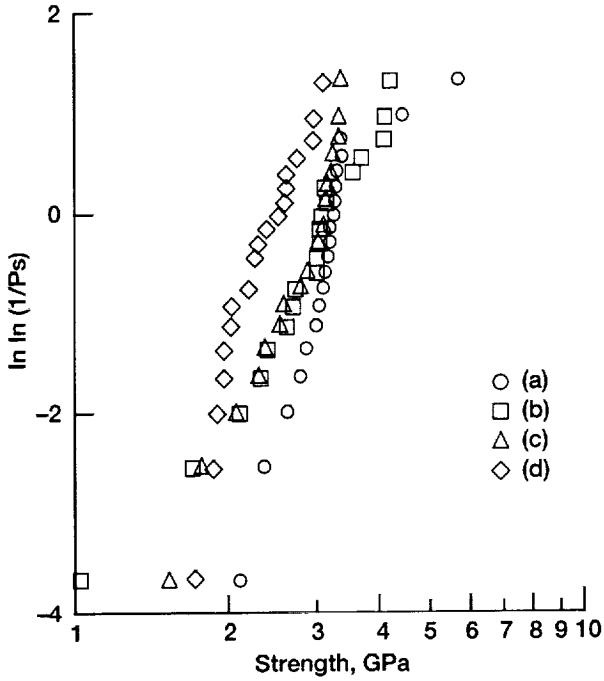

Figure 15.—Weibull probability plots for room temperature tensile strengths of (a) Hi-Nicalon, (b) Hi-Nicalon/$LaPO_4$, (c) Sylramic, and (d) Sylramic/$LaPO_4$ fibers.

TABLE II. WEIBULL PARAMETERS FOR ROOM TEMPERATURE TENSILE STRENGTH OF HI-NICALON AND SYLRAMIC FIBERS

Fiber	Average strength, GPa	Std. dev., GPa	Weibull modulus, m
Hi-Nicalon (as-received, flame desized)	3.19	0.73	5.41
Monazite coated Hi-Nicalon	2.91	0.78	3.75
Sylramic (as-received, flame desized)	2.78	0.53	5.52
Monazite coated Sylramic	2.33	0.39	7.13

20 filaments tested for each fiber type: gage length = 2.54 cm; crosshead speed = 1.261 mm/min.

An average diameter of 13.5 μm for Hi-Nicalon and 10.8 μm for Sylramic fibers was used.

5. SUMMARY

Room temperature tensile strengths of as-received Hi-Nicalon and Sylramic fibers and those having monazite surface coatings were measured. The average tensile strengths of uncoated Hi-Nicalon and Sylramic fibers were 3.19±0.73 and 2.78±0.53 GPa with a Weibull modulus of 5.41 and 5.52, respectively. The Hi-Nicalon and Sylramic fibers coated with monazite surface layers showed strength loss of ~10 and 15 percent, respectively. The elemental compositions of the fibers and the coatings were analyzed using scanning Auger microprobe and EDS. The $LaPO_4$ coating on Hi-Nicalon fibers was about 50 nm thick and approximately stoichiometric. The coating on the Sylramic fibers extended to a depth of about 100 to 150 nm. The coating may have been stoichiometric $LaPO_4$ in the first 30 to 40 nm of the layer. However, the surface roughness of Sylramic fiber made this profile very difficult to interpret. Microstructural analyses of the fibers and the coatings were done by SEM, TEM, and selected area electron diffraction. Hi-Nicalon fiber consists of fine β-SiC nanocrystals ranging in size from 1 to 30 nm embedded in an amorphous matrix. Sylramic is a polycrystalline stoichiometric silicon carbide fiber consisting of submicron β-SiC crystallites ranging from 100 to 300 nm. Small amount of TiB_2 nanocrystallites (~50 nm) are also present. The $LaPO_4$ coating on Hi-Nicalon fibers consisted of a chain of peanut shape particles having monazite-(La) structure. The coating on Sylramic fibers consisted of two layers. The inner layer was a chain of peanut shape particles having monazite-(La) structure while the outer layer comprised of much smaller microcrystalline particles.

6. CONCLUSIONS AND FUTURE WORK

Application of monazite surface coatings on Hi-Nicalon and Sylramic fibers degrade their room temperature tensile strength by ~10 and 15 percent, respectively. The monazite-coated silicon carbide fibers will be used as reinforcement for celsian and other matrix composites.

REFERENCES

1. J.J. Brennan, Glass and Glass-Ceramic Matrix Composites, in Fiber-Reinforced Ceramic Composites (K. S. Mazdiyasni, Editor), Noyes, Park Ridge, NJ, 1990, pp. 222–259.
2. N.P. Bansal, "Strong and Tough Hi-Nicalon Fiber-Reinforced Celsian Matrix Composites," *J. Am. Ceram. Soc.*, **80** [9], pp. 2407–2409 (1997).
3. N.P. Bansal and J.I. Eldride, "Hi-Nicalon Fiber-Reinforced Celsian Matrix Composites: Influence of Interface Modification," *J. Mater. Res.*, **13**[6], pp. 1530–1537 (1998).
4. N.P. Bansal, Ceramic Fiber-Reinforced Glass-Ceramic Matrix Composites, U.S. Patent No. 5,214,004, May 25, 1993.
5. A.W. Moore, H. Sayir, S.C. Farmer, and G.N. Morscher, "Improved Interface Coatings for SiC Fibers in Ceramic Composites," *Ceram. Eng. Sci. Proc.*, **16**[4], pp. 409–416 (1995).
6. P.E.D. Morgan and D.B. Marshall, "Functional Interfaces for Oxide/Oxide Composites," *Mater. Sci. Eng.*, **A162** [1–2], pp. 15–25 (1993).
7. M.K. Cinibulk, "Synthesis of Calcium Hexaluminate and Lanthanum Hexaluminate Fiber Coatings," *Ceram. Eng. Sci. Proc.*, **19**[3], pp. 27–35 (1998).
8. P.V. Chayka, "Liquid MOCVD Precursors and Their Application to Fiber Interface Coatings," *Ceram. Eng. Sci. Proc.*, **18**[3], pp. 287–294 (1997).
9. A. Cazzato, M. Colby, D. Daws, J. Davis, P. Morgan, J. Porter, S. Butner, and B. JURF, "Monazite Interface Coatings in Polymer and Sol-Gel Derived Ceramic Matrix Composites," *Ceram. Eng. Sci. Proc.*, **18**[3], pp. 269–278 (1997).
10. R.W. Goettler, S. Sambasivan, and V.P. Dravid, "Isotropic Complex Oxides as Fiber Coatings for Oxide-Oxide CFCC," *Ceram. Eng. Sci. Proc.*, **18**[3], pp. 279–286 (1997).
11. E. Boakye, R.S. Hay, and M.D. Petry, "Continuous Coating of Oxide Fiber Tows Using Liquid Precursors: Monazite Coatings on Nextel 720™," *J. Am. Ceram. Soc.*, **82**[9], pp. 2321–2331 (1999).
12. T.A. Parthasarathy, E. Boakye, M.K. Cinibulk, and M.D. Petry, "Fabrication and testing of Oxide/Oxide Microcomposites with Monazite and Hibonite as Interlayers," *J. Am. Ceram. Soc.*, **82**[12], pp. 3575–3583 (1999).

13. J.R. Mawdsley, D. Kovar, and J.W. Halloran, "Fracture Behavior of Alumina/Monazite Multilayer Laminates," *J. Am. Ceram. Soc.*, **83**[4], pp. 802–808 (2000).
14. N.P. Bansal and R.M. Dickerson, "Tensile Strength and Microstructural Characterization of HPZ Ceramic Fibers," *Mater. Sci. Eng.*, **A222** [2], pp. 149–157 (1997).
15. N.P. Bansal, "Effects of HF Treatments on Tensile Strengths of Hi-Nicalon Fibers", *J. Mater. Sci.*, **33**[17] pp. 4287–4295 (1998).
16. N.P. Bansal and Y.L. Chen, "Chemical, Mechanical and Microstructural Characterization of Low-Oxygen Containing Silicon Carbide Fibers with Ceramic Coatings," *J. Mater. Sci.*, **33**[22] pp. 5277–5289 (1998).
17. G. Chollen, R. Pailler, R. Naslain, and P. Olry, "Correlation Between Microstructure and Mechanical Behavior at High Temperatures of a SiC Fiber with a Low Oxygen Content (Hi-Nicalon)," *J. Mater. Sci.*, **32** [5], pp. 1133–1147 (1997).
18. T. Shimoo, I. Tsukada, M. Narisawa, T. Seguchi, and K. Okamura, "Change in Properties of Polycarbosilane-Derived SiC Fibers at High Temperatures," *J. Ceram. Soc. Jpn.*, **105** [7], pp. 559–563 (1997).
19. W.A. Weibull, "A Statistical Distribution Function of Wide Applicability," *J. Appl. Mech.*, **18** [9], pp. 293–297 (1951).
20. S. Van Der Zwaag, "The Concept of Filament Strength and the Weibull Modulus," *J. Testing Eval.*, **17** [5], pp. 292–298 (1989).
21. M.D. Petry, T.-I. Mah, and R.J. Kerans, "Validity of Using Average Diameter for Determination of Tensile Strength and Weibull Modulus of Ceramic Filaments," *J. Am. Ceram. Soc.*, **80** [10], pp. 2741–2744 (1997).
22. J. Hurst, H.-M. Yun, and D. Gorican, "A Comparison of the Mechanical Properties of Three Polymer-Derived Small Diameter SiC Fibers," in *Advances in Ceramic Matrix Composites III*, (N.P. Bansal and J.P. Singh, Editors), Am. Ceram. Soc., Westerville, OH; *Ceram. Trans.*, **74**, pp. 3–15 (1996).
23. M. Takeda, J. Sakamoto, A. Saeki, and H. Ichikawa, "High Performance Silicon Carbide Fiber Hi-Nicalon for Ceramic Matrix Composites," *Ceram. Eng. Sci. Proc.*, **16**[4], pp. 37–44 (1995).

REPORT DOCUMENTATION PAGE

Form Approved
OMB No. 0704-0188

1. AGENCY USE ONLY (*Leave blank*)	2. REPORT DATE	3. REPORT TYPE AND DATES COVERED
	June 2000	Technical Memorandum

4. TITLE AND SUBTITLE

Mechanical, Chemical and Microstructural Characterization of Monazite-Coated Silicon Carbide Fibers

5. FUNDING NUMBERS

WU–523–31–13–00

6. AUTHOR(S)

N.P. Bansal, D.R. Wheeler, and Y.L. Chen

7. PERFORMING ORGANIZATION NAME(S) AND ADDRESS(ES)

National Aeronautics and Space Administration
John H. Glenn Research Center at Lewis Field
Cleveland, Ohio 44135–3191

8. PERFORMING ORGANIZATION REPORT NUMBER

E–12328

9. SPONSORING/MONITORING AGENCY NAME(S) AND ADDRESS(ES)

National Aeronautics and Space Administration
Washington, DC 20546–0001

10. SPONSORING/MONITORING AGENCY REPORT NUMBER

NASA TM—2000-210208

11. SUPPLEMENTARY NOTES

N.P. Bansal and D.R. Wheeler, NASA Glenn Research Center; Y.L. Chen, Dynacs Engineering Company, Inc., 2001 Aerospace Parkway, Brook Park, Ohio 44142. Responsible person, Narottam P. Bansal, organization code 5130, (216) 433–3855.

12a. DISTRIBUTION/AVAILABILITY STATEMENT

Unclassified - Unlimited
Subject Category: 27 Distribution: Nonstandard

This publication is available from the NASA Center for AeroSpace Information, (301) 621–0390.

12b. DISTRIBUTION CODE

13. ABSTRACT (*Maximum 200 words*)

Tensile strengths of as-received Hi-Nicalon and Sylramic fibers and those having monazite surface coatings, deposited by atmospheric pressure chemical vapor deposition, were measured at room temperature and the Weibull statistical parameters determined. The average tensile strengths of uncoated Hi-Nicalon and Sylramic fibers were 3.19±0.73 and 2.78±0.53 GPa with a Weibull modulus of 5.41 and 5.52, respectively. The monazite-coated Hi-Nicalon and Sylramic fibers showed strength loss of ~10 and 15 percent, respectively, compared with the as-received fibers. The elemental compositions of the fibers and the coatings were analyzed using scanning Auger microprobe and energy dispersive x-ray spectroscopy. The $LaPO_4$ coating on Hi-Nicalon fibers was approximately stoichiometric and about 50 nm thick. The coating on the Sylramic fibers extended to a depth of about 100 to 150 nm. The coating may have been stoichiometric $LaPO_4$ in the first 30 to 40 nm of the layer. However, the surface roughness of Sylramic fiber made this profile somewhat difficult to interpret. Microstructural analyses of the fibers and the coatings were done by scanning electron microscopy, transmission electron microscopy, and selected area electron diffraction. Hi-Nicalon fiber consists of fine β-SiC nanocrystals ranging in size from 1 to 30 nm embedded in an amorphous matrix. Sylramic is a polycrystalline stoichiometric silicon carbide fiber consisting of submicron β-SiC crystallites ranging from 100 to 300 nm. Small amount of TiB_2 nanocrystallites (~50 nm) are also present. The $LaPO_4$ coating on Hi-Nicalon fibers consisted of a chain of peanut shape particles having monazite-(La) structure. The coating on Sylramic fibers consisted of two layers. The inner layer was a chain of peanut shape particles having monazite-(La) structure. The outer layer was comprised of much smaller particles with a microcrystalline structure.

14. SUBJECT TERMS

SiC fibers; Hi-Nicalon; Sylramic; Monazite; Microscopy; Tensile strength; Microstructure

15. NUMBER OF PAGES
25

16. PRICE CODE
A03

17. SECURITY CLASSIFICATION OF REPORT	18. SECURITY CLASSIFICATION OF THIS PAGE	19. SECURITY CLASSIFICATION OF ABSTRACT	20. LIMITATION OF ABSTRACT
Unclassified	Unclassified	Unclassified	